

Floating-Ring Bearings Dynamic Force Coefficients Identification: Measurement and Prediction

Daniel Tamunodukobipi^a. Yong-Bok Lee^b. Ezenwa Ogbonnaya^c

^aDepartment of Marine Engineering, Rivers State University of Science and Technology, Port Harcourt, Nigeria,

^bEnergy Mechanics Resource Center, Korea Institute of Science and Technology, 39-1 Hawolgok-dong, Songbuk-gu, Seoul, 136-791, Korea

^cDepartment of Marine/Mechanical Engineering, Niger Delta University, Wilberforce Island, Yenagoa, Bayelsa State, Nigeria,

Abstract: Identification of floating-ring bearings (FRBs) dynamic force coefficients has not been well documented because of properties' non-linearity, measurement complexity and predictive inaccuracy. This paper presents techniques for quantitative analysis and experimental characterization of FRB dynamic parameters. A four-degree-of-freedom (4-D.O.F) system algorithm is developed and implemented using analytically obtained inner and outer films' force coefficients. The results show a general rise in stiffness and damping coefficients with speed except K_{yy} which has a negative gradient. It is found that FRB low-frequency instability is essentially caused by large negative K_{xy} , created by weak outer oil-film hydrodynamic wedge. The monotonical increase in damping and direct stiffness K_{xx} due to improved outer-film hydrodynamics enhances FRB high-speed performance. However, measurement inconsistency ensued at very high speed because of increased boundary-lubrication. Both measurements and predictions are comparatively in good agreement.

Key Words: floating-ring bearing; dynamic coefficients; analytical modeling; oil-bearing.

I. INTRODUCTION

Floating-ring bearing (FRB) structurally possesses a cylindrical metal ring (floating-ring) loosely fitted between the journal and the bearing housing. The ring becomes fluid borne on spinning under viscous shear to constitute two parallel hydrodynamic oil-films that act in series [1-3]. Figure 1 shows a schematic of a full floating-ring bearing (FRB). This bearing is an improved version of the traditional single film journal bearing (JB) and the more recent semi floating-ring bearing (SFRB) as indicated in Figure 2. FRBs are widely applied in turbochargers, micro gas-turbines, air cycle machines, and turbo-compressors [2, 4, 5]. Their broad implementation in comparison to conventional JBs is due to the following: (a) low procurement cost, (b) low friction and easy to replace, (c) higher hydrodynamic stability and damping, (d) better convective cooling and thermal management, (e) greater tolerance to misalignment, distortion and expansion, and (f) better bearing performance at off-design conditions [1-5]. Evidently, FRB is probably the most common low-friction bearing for high-speed turbomachinery. Therefore, a research study for its parameters characterization becomes imperative for optimal design and reliable operation of this category of rotor-bearing systems.

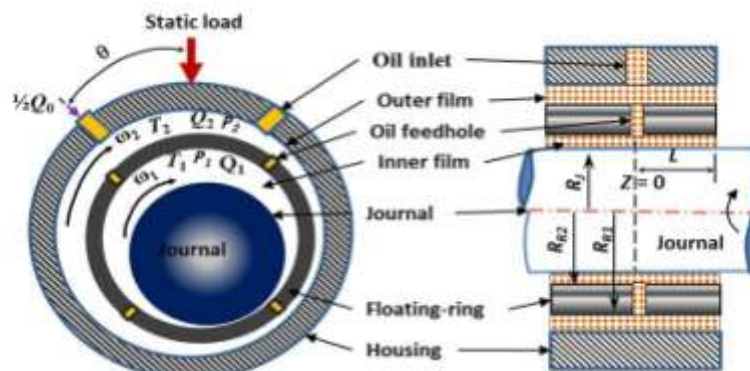


Fig. 1 Description of a full floating-ring bearing (FRB), showing the major features

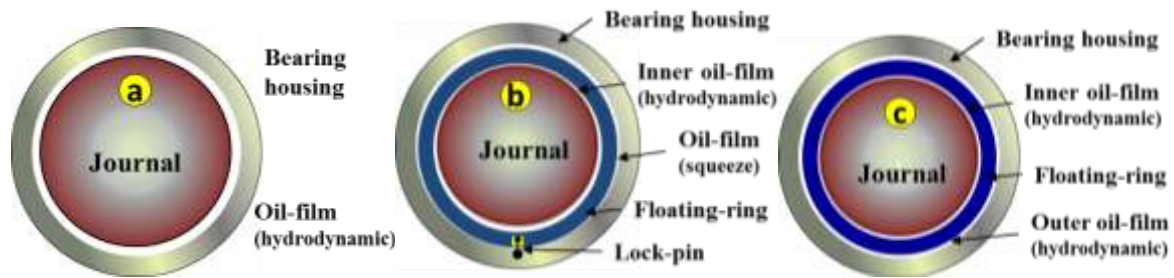


Fig. 2 Basic types of oil-film JBs (a) conventional JB, (b) semi FRB, and (c) full FRB

1.1 Research Background

Floating-ring bearings (FRBs) force coefficients are functions of bearing geometry, rotor motions (speeds and eccentricities) and lubricant properties [1-3]. Properly characterized dynamic force coefficients of FRB oil-films are very necessary for estimating rotor's load-bearing capacity, critical speed, unbalance response and threshold speed of instability [1, 4]. Major setbacks of parameters identification for this class of *JBs* are due to: (a) the inadequacies of contemporary theories to provide reliable and comprehensive analysis of FRB parameters; and (b) the insufficient availability of published test data to validate and benchmark predictive models. Some inherent uncertainties in FRB theory exist, particularly in the areas of boundary conditions, film cavitation, subsynchronous whirl phenomenon and non-linearity of film forces [5, 6]. These shortfalls mar the dependability of FRB dynamic-force-coefficient predictors, and consequently accentuate the need for reliable test-data to benchmark and calibrate extant predictive models. Figure 3 presents a turbocharger rotor supported on FRBs.

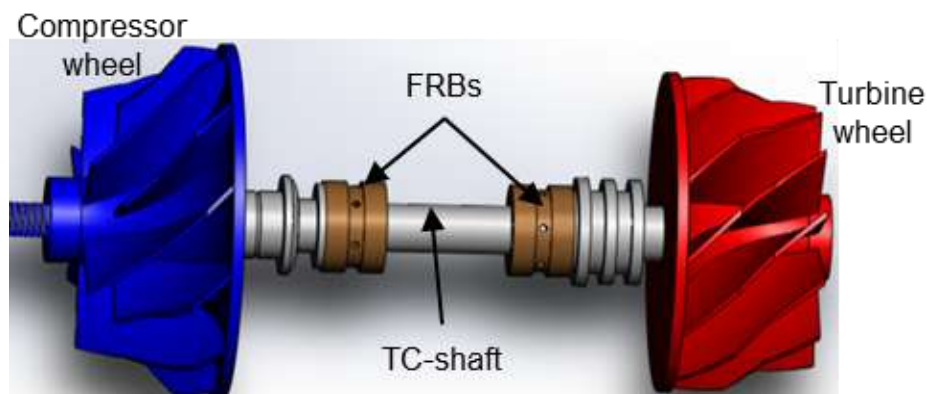


Fig. 3 Floating-ring bearing supported turbocharger shaft

II. PREVIOUS CONTRIBUTIONS

Over the years, FRB dynamic force coefficients characterization has been an exclusive workshop practice because most thin-film models are considered poor representatives of candidate bearings [6, 7]. Typical measurement becomes imperative even though data quality is sometimes undermined by sub-synchronous instability, electromechanical noise, rubbing, and thermal induced variation in film clearances [8, 9]. Shaw and Nussdorfer [1] performed analytical study on the operating characteristics of a fully floating-ring bearing. Results of ring-to-journal speed ratio (Ω_2/Ω_1), mean radial clearance ratio (C_2/C_1) and FRB comparative energy dissipation capability were presented in tandem with those for a conventional single-film *JB* of equivalent geometric parameters. It was found that, for same viscosity (μ) of oil, the values of Ω_2/Ω_1 and the bearing friction loss depended largely on the quantity C_2/C_1 . Thus, it was established that FRB has superior low-friction and better heat-dissipation performance than conventional *JBs*. Born [2] further investigated the influence of C_2/C_1 on FRB dynamic load bearing capacity and its threshold speed of instability, particularly for a FRB borne turbocharger (*TC*) rotor. Born revealed that *TC* stability improved considerably when the inner film clearance got narrower: a finding which is consistent with the test results of References [1, 3, 7, 10]. Holt and San Andrés [4, 5] examined the effects of casing acceleration on a FRB supported automotive *TC* with a peak speed of 115,000 *rpm*. Results of their linear and non-linear rotordynamic models closely predicted test data on dynamic force responses, critical speed, onset speed of instability, and transient response of the test rotor-bearing system. In addition, the authors demonstrated analytically the prevalence of at least two sub-synchronous instabilities which characteristically occurred at 50% of ring speed; and 50% of the sum of ring and journal speeds,

respectively. Note that most of the research papers referenced in this section are fundamentally on FRB stability analysis, ring motion and bearing friction losses.

Consequently, Orcutt and Ng [11], and Chow [8] considered the analysis of FRB dynamic force coefficients characterization at steady-state perturbation with pressurized lubricant supply. In their separate piecewise numerical integrations, based on Lund’s model [12] for short *JBs*, the researchers obtained sixteen linearized dynamic force parameters from the two oil-films. These were subsequently condensed to the standard eight non-dimensional force coefficients using force balancing algorithm. Their analytical results, however, were not authenticated by measurement. On the other hand, Tamunodukobipi, et al [6, 9] experimentally investigated the dynamic performance characterization of *FRBs* with varied oil-injection angles for attenuating hydrodynamic instability. In that work, practical techniques for FRB dynamic force coefficients identification, rotor-bearing instability response minimization, and ring-to-journal dynamic parameters (Ω_2/Ω_1 , μ_2/μ_1 , C_2/C_1) evaluations were laid down. Reliable and comprehensive test data for FRB dynamic load capacities, damping performance and response behavior were presented; but the authors did not show any correlation with simulated data.

Correlation of predictions with measurements of FRB dynamic properties is still uncommon, despite the long history of this class of bearings. Even where such exists, the reliability is impaired by unresolved uncertainties [6]. Such snags are evidently so, because *FRBs* exhibit unusual dynamic behaviors which are not effectively characterized by canonical *JB* theory. Until now, only experimentally identified dynamic parameters have proven to be reliable [6]. In addition, the fabricating and dynamic testing of *FRBs* are expensive, time-consuming and tedious undertaking. Thus, using model predictors becomes invariably a swifter, more economical, easier to implement and more adaptive means of bearing characterization. Well formulated models are readily adopted as subroutines for larger programs. In view of their relevance, this work presents model predictors for characterizing FRB dynamic force coefficients; and benchmarks their predictions against test data. The research employs modified hydrodynamic bearing relations, theory of force balancing and piecewise integration technique as basis for its modeling. Graphic correlations of test and simulated data are presented and succinctly elucidated. The contents of this work may be valuable for preliminary design of *FRBs*, estimating their stiffness and damping properties, and predicting their dynamic behaviors. The models developed could be useful for parametric study, and prognostic analyses of FRB supported rotor systems.

III. DYNAMIC PARAMETERS IDENTIFICATION MODELING

This section models FRB as a four-degree-of-freedom (*4-D.O.F*) system and implements force balance on the ring and the housing respectively, as shown in Figure 4. The fixed reference is the journal which is assumed to have no lateral displacement. This is valid for a well balanced rigid rotor supported on ball bearings. The 2-mass-spring-damper system is divided into the floating-ring (m_R) which is under the influence of the inner and outer film forces; and the housing (m_H) that is supported wholly on the outer film.

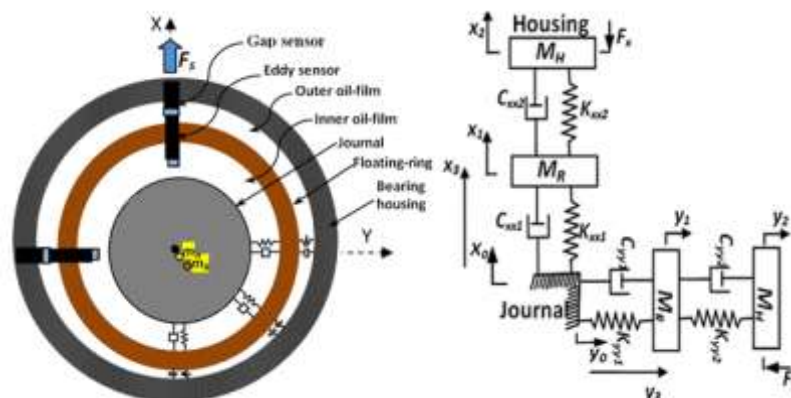


Fig. 4 Schematics of FRB, showing the two-film forces and sensors arrangement

Let $\{X_0 e^{i\omega t}, Y_0 e^{i\omega t}\}$, $\{X_1 e^{i\omega t}, Y_1 e^{i\omega t}\}$ and $\{X_2 e^{i\omega t}, Y_2 e^{i\omega t}\}$ be the displacements of journal (*J*), floating-ring (*R*) and housing (*H*) from their steady-state equilibrium positions after impact, respectively. Equation of their relative displacements is

$$\begin{Bmatrix} X_2 - X_0 \\ Y_2 - Y_0 \end{Bmatrix} e^{i\omega t} = \begin{Bmatrix} X_2 - X_1 \\ Y_2 - Y_1 \end{Bmatrix} e^{i\omega t} + \begin{Bmatrix} X_1 - X_0 \\ Y_1 - Y_0 \end{Bmatrix} e^{i\omega t} \tag{1}$$

which is redefined concisely as:

$$\begin{Bmatrix} x_3 \\ y_3 \end{Bmatrix} = \begin{Bmatrix} x_2 \\ y_2 \end{Bmatrix} + \begin{Bmatrix} x_1 \\ y_1 \end{Bmatrix} \tag{2}$$

Force balance operation on the floating-ring mass-spring-damper system yields Eq. (3). On impact loading, the instantaneous compressive force transmitted through the outer film to the floating-ring and is countered by the inner film dynamic stiffness designated as $[d_{(\omega)}^{in}]$

$$\begin{bmatrix} d_{xx}^{in} & d_{xy}^{in} \\ d_{yx}^{in} & d_{yy}^{in} \end{bmatrix} \begin{Bmatrix} x_1 \\ y_1 \end{Bmatrix} = \begin{bmatrix} K_{xx2} + i\omega C_{xx2} & K_{xy2} + i\omega C_{xy2} \\ K_{yx2} + i\omega C_{yx2} & K_{yy2} + i\omega C_{yy2} \end{bmatrix} \begin{Bmatrix} x_2 \\ y_2 \end{Bmatrix} \tag{3}$$

$$\begin{Bmatrix} x_1 \\ y_1 \end{Bmatrix} = \begin{bmatrix} d_{xx}^{in} & d_{xy}^{in} \\ d_{yx}^{in} & d_{yy}^{in} \end{bmatrix}^{-1} \begin{bmatrix} K_{xx2} + i\omega C_{xx2} & K_{xy2} + i\omega C_{xy2} \\ K_{yx2} + i\omega C_{yx2} & K_{yy2} + i\omega C_{yy2} \end{bmatrix} \begin{Bmatrix} x_2 \\ y_2 \end{Bmatrix} \tag{4}$$

Equally, the housing displaces toward the floating-ring, but its motion is resisted by the reaction forces ensuing from the outer film relative dynamic stiffness, as given in equation (5)

$$\begin{bmatrix} d_{xx}^{out} & d_{xy}^{out} \\ d_{yx}^{out} & d_{yy}^{out} \end{bmatrix} \begin{Bmatrix} x_2 \\ y_2 \end{Bmatrix} + \begin{bmatrix} -\omega^2 M_{xxH} & -\omega^2 M_{xyH} \\ -\omega^2 M_{yxH} & -\omega^2 M_{yyH} \end{bmatrix} \begin{Bmatrix} x_1 \\ y_1 \end{Bmatrix} = \begin{Bmatrix} F_{xH} \\ F_{yH} \end{Bmatrix} \tag{5}$$

$[d_{(\omega)}^{out}]$ is the outer-film force matrix. Combining Eqs (4) and (5) gives

$$\begin{Bmatrix} F_{xH} \\ F_{yH} \end{Bmatrix} = \begin{pmatrix} \begin{bmatrix} -\omega^2 M_{xxH} & -\omega^2 M_{xyH} \\ -\omega^2 M_{yxH} & -\omega^2 M_{yyH} \end{bmatrix} \begin{bmatrix} d_{xx}^{in} & d_{xy}^{in} \\ d_{yx}^{in} & d_{yy}^{in} \end{bmatrix}^{-1} \\ \begin{bmatrix} K_{xx2} + i\omega C_{xx2} & K_{xy2} + i\omega C_{xy2} \\ K_{yx2} + i\omega C_{yx2} & K_{yy2} + i\omega C_{yy2} \end{bmatrix} + \begin{bmatrix} d_{xx}^{out} & d_{xy}^{out} \\ d_{yx}^{out} & d_{yy}^{out} \end{bmatrix} \end{pmatrix} \begin{Bmatrix} x_2 \\ y_2 \end{Bmatrix} \tag{6}$$

The terms in the round bracket represent obviously the FRB dynamic stiffness $[D_{(\omega)}^{eq}]$. In Eq. (4), when $\begin{Bmatrix} x_1 \\ y_1 \end{Bmatrix}$

approaches zero, then $[d_{(\omega)}^{in}]$ tends to be infinitely large. Such condition prevails at extremely high speed with the apparent disappearance of inner film clearance due to thermal expansion and centrifugal growth. The floating-ring attaches itself to the shaft in the absence of inner-film to form a rotor-disc. Knowing that the film forces are not pure but have cross-coupling effects: equation (6) can be rewritten as

$$\begin{bmatrix} F_{xx}^{eq} & F_{xy}^{eq} \\ F_{yx}^{eq} & F_{yy}^{eq} \end{bmatrix} = \begin{pmatrix} \begin{bmatrix} -\omega^2 M_{xxH} & -\omega^2 M_{xyH} \\ -\omega^2 M_{yxH} & -\omega^2 M_{yyH} \end{bmatrix} \begin{bmatrix} d_{xx}^{in} & d_{xy}^{in} \\ d_{yx}^{in} & d_{yy}^{in} \end{bmatrix}^{-1} \\ \begin{bmatrix} K_{xx2} + i\omega C_{xx2} & K_{xy2} + i\omega C_{xy2} \\ K_{yx2} + i\omega C_{yx2} & K_{yy2} + i\omega C_{yy2} \end{bmatrix} + \begin{bmatrix} d_{xx}^{out} & d_{xy}^{out} \\ d_{yx}^{out} & d_{yy}^{out} \end{bmatrix} \end{pmatrix} \begin{bmatrix} X_{xx} & X_{xy} \\ X_{yx} & X_{yy} \end{bmatrix} \tag{7}$$

Dividing equation (7) by the displacement matrix $[X]$, yields

$$\begin{bmatrix} F_{xx}^{eq} & F_{xy}^{eq} \\ F_{yx}^{eq} & F_{yy}^{eq} \end{bmatrix} \begin{bmatrix} X_{xx} & X_{xy} \\ X_{yx} & X_{yy} \end{bmatrix}^{-1} = \begin{pmatrix} \begin{bmatrix} -\omega^2 M_{xxH} & -\omega^2 M_{xyH} \\ -\omega^2 M_{yxH} & -\omega^2 M_{yyH} \end{bmatrix} \begin{bmatrix} d_{xx}^{in} & d_{xy}^{in} \\ d_{yx}^{in} & d_{yy}^{in} \end{bmatrix}^{-1} \\ \begin{bmatrix} K_{xx2} + i\omega C_{xx2} & K_{xy2} + i\omega C_{xy2} \\ K_{yx2} + i\omega C_{yx2} & K_{yy2} + i\omega C_{yy2} \end{bmatrix} + \begin{bmatrix} d_{xx}^{out} & d_{xy}^{out} \\ d_{yx}^{out} & d_{yy}^{out} \end{bmatrix} \end{pmatrix}$$

Thus, the FRB dynamic coefficients matrix can be expressed as

$$\begin{bmatrix} d_{xx}^{eq} & d_{xy}^{eq} \\ d_{yx}^{eq} & d_{yy}^{eq} \end{bmatrix} = \begin{pmatrix} \begin{bmatrix} -\omega^2 M_{xxH} & -\omega^2 M_{xyH} \\ -\omega^2 M_{yxH} & -\omega^2 M_{yyH} \end{bmatrix} \begin{bmatrix} d_{xx}^{in} & d_{xy}^{in} \\ d_{yx}^{in} & d_{yy}^{in} \end{bmatrix}^{-1} \\ \begin{bmatrix} K_{xx2} + i\omega C_{xx2} & K_{xy2} + i\omega C_{xy2} \\ K_{yx2} + i\omega C_{yx2} & K_{yy2} + i\omega C_{yy2} \end{bmatrix} + \begin{bmatrix} d_{xx}^{out} & d_{xy}^{out} \\ d_{yx}^{out} & d_{yy}^{out} \end{bmatrix} \end{pmatrix} \tag{8}$$

The inner and outer films have distinctive hydrodynamic behavior, and their force coefficients should be separately determined. In this work the force coefficients are obtained by piecewise linear integrations of film pressure forces at steady-state as given Eqs. (9) and (10). Short bearing theory is incorporated in this analysis and oil-film ruptures in both films at low speeds are neglected. However, at high speed, film rupture effect is considered for the inner film: since centrifugal repulsion and high temperature promote the forming of bubbles.

$$\left\{ \begin{array}{l} K_{xx} = \frac{\partial F_x}{\partial x} \quad ; \quad K_{xy} = \frac{\partial F_x}{\partial y} \\ K_{yx} = \frac{\partial F_y}{\partial x} \quad ; \quad K_{yy} = \frac{\partial F_y}{\partial y} \end{array} \right. \quad \text{and} \quad \left\{ \begin{array}{l} C_{xx} = \frac{\partial F_x}{\partial \dot{x}} \quad ; \quad C_{xy} = \frac{\partial F_x}{\partial \dot{y}} \\ C_{yx} = \frac{\partial F_y}{\partial \dot{x}} \quad ; \quad C_{yy} = \frac{\partial F_y}{\partial \dot{y}} \end{array} \right.$$

$$\left[\begin{array}{cc} K_{xx} & K_{xy} \\ K_{yx} & K_{yy} \end{array} \right] = 2 \left[\begin{array}{cc} \int_0^{a_i+\pi} \int_0^{1/2} P_x r \cos \theta \, \partial z \, \partial \theta & \int_0^{a_i+\pi} \int_0^{1/2} P_y r \cos \theta \, \partial z \, \partial \theta \\ \int_0^{a_i+\pi} \int_0^{1/2} P_x r \sin \theta \, \partial z \, \partial \theta & \int_0^{a_i+\pi} \int_0^{1/2} P_y r \sin \theta \, \partial z \, \partial \theta \end{array} \right] \quad (9)$$

$$\left[\begin{array}{cc} C_{xx} & C_{xy} \\ C_{yx} & C_{yy} \end{array} \right] = 2 \left[\begin{array}{cc} \int_0^{a_i+\pi} \int_0^{1/2} P_x r \cos \theta \, \partial z \, \partial \theta & \int_0^{a_i+\pi} \int_0^{1/2} P_y r \cos \theta \, \partial z \, \partial \theta \\ \int_0^{a_i+\pi} \int_0^{1/2} P_x r \sin \theta \, \partial z \, \partial \theta & \int_0^{a_i+\pi} \int_0^{1/2} P_y r \sin \theta \, \partial z \, \partial \theta \end{array} \right] \quad (10)$$

Film viscosities and clearances are dependent on the effective local temperature in each film and the shear rate, $\dot{\gamma}$. The variation of viscosity in a non-Newtonian lubricant is accurately estimated by using a modified model of Cross and Vogel's equations, Taylor [13, 14].

$$\mu = \left\{ \mu_\infty - \frac{\mu_\infty - K e^{a/(b+T)}}{\left(\frac{\dot{\gamma}}{\dot{\gamma}_c} \right)} \right\} \quad [11]$$

Where μ_∞ represents reference viscosity at null shear rate; while K , a and b are Vogel' thermo-viscous fitting parameters to be determined experimentally; while $\dot{\gamma}$ and $\dot{\gamma}_c$ are the shear rate and the shear rate that produces 50% reduction in reference viscosity, respectively. In this analysis, well modeled temperature dependent fluid-film clearance and viscosity ratios (with shear thinning effect) are employed for computing the FRB dynamic force parameters.

Characteristically, FRB performance is highly sensitive to bearing geometry and lubricant properties, References [1-5]. At steady-state, floating-ring angular acceleration is zero. The Sommerfeld numbers for the inner and outer films are defined in Eq. (12).

$$\text{Sommerfeld No} = \left[\begin{array}{l} Sn_1 = \frac{\mu_1 (\Omega_J - \Omega_R) LD_1}{W_1} \left(\frac{R_1}{c_1} \right)^2 \\ Sn_2 = \frac{\mu_2 \Omega_R LD_2}{W_2} \left(\frac{R_2}{c_2} \right)^2 = \left[\frac{\alpha}{1 + \alpha} \left(\frac{\mu_2}{\mu_1} \right) \left(\frac{R_2}{R_1} \right)^3 \left(\frac{C_1}{C_2} \right)^2 S_1 \right]_{\alpha = (\Omega_R / \Omega_J)} \end{array} \right] \quad (12)$$

From the Sommerfeld numbers, the ring-to-journal speed ratio (α) is derived as:

$$\frac{Sn_2}{Sn_1} = \frac{\Omega_R}{(\Omega_J - \Omega_R)} \left(\frac{\mu_2}{\mu_1} \right) \left(\frac{P_1}{P_2} \right) \left(\frac{c_1}{c_2} \right)^2 \left(\frac{R_2}{R_1} \right)^3 = \lambda_s \left(\frac{\epsilon_1}{\epsilon_2} \right) \left(\frac{1 - \epsilon_2^2}{1 - \epsilon_1^2} \right)^2 \sqrt{\frac{16 \epsilon_1^2 + \pi^2 (1 - \epsilon_1^2)}{16 \epsilon_2^2 + \pi^2 (1 - \epsilon_2^2)}}$$

$$\frac{\alpha}{(1 - \alpha)} \left(\frac{\mu_2}{\mu_1} \right) \left(\frac{c_1}{c_2} \right)^2 \left(\frac{P_1}{P_2} \right) \left(\frac{R_2}{R_1} \right)^3 = \lambda_\epsilon \left(\frac{\epsilon_1}{\epsilon_2} \right) \left(\frac{1 - \epsilon_2^2}{1 - \epsilon_1^2} \right)^2 \sqrt{\frac{16 \epsilon_1^2 + \pi^2 (1 - \epsilon_1^2)}{16 \epsilon_2^2 + \pi^2 (1 - \epsilon_2^2)}}$$

$$\alpha = \left(\frac{\lambda_\alpha \left(\frac{\varepsilon_1}{\varepsilon_2} \right) \left(\frac{1 - \varepsilon_2^2}{1 - \varepsilon_1^2} \right)^2 \sqrt{16 \varepsilon_1^2 + \pi^2 (1 - \varepsilon_1^2)}}{\left(\frac{\mu_2}{\mu_1} \right) \left(\frac{P_1}{P_2} \right) \left(\frac{c_1}{c_2} \right)^2 \left(\frac{R_2}{R_1} \right)^3 + \left(\frac{\varepsilon_1}{\varepsilon_2} \right) \left(\frac{1 - \varepsilon_2^2}{1 - \varepsilon_1^2} \right)^2 \sqrt{16 \varepsilon_1^2 + \pi^2 (1 - \varepsilon_1^2)}} \right) \quad (13)$$

$$\text{where : } \begin{cases} \text{subscript } (i) & = \begin{cases} 1 \rightarrow \text{inner bearing} \\ 2 \rightarrow \text{outer bearing} \end{cases} \\ \text{bearing load} & = \begin{cases} W_1 = \frac{\mu_1 R_1 \Omega_j \varepsilon_1 L^3}{4 C_1^2 (1 - \varepsilon_1^2)^2} \sqrt{16 \varepsilon_1^2 + \pi^2 (1 - \varepsilon_1^2)} \\ W_2 = \frac{\mu_2 R_2 \Omega_r \varepsilon_2 L^3}{4 C_2^2 (1 - \varepsilon_2^2)^2} \sqrt{16 \varepsilon_2^2 + \pi^2 (1 - \varepsilon_2^2)} \end{cases} \end{cases}$$

where $(P=W/LD)$, $(\varepsilon_1= e_1/c_1)$ and $(\varepsilon_2= e_2/c_2)$ are the bearing load, inner film eccentricity and outer film eccentricity, respectively. λ_α and λ_ε represent the correlation factors for speed ratio and eccentricity ratio, respectively. λ_α is a function of the applied load, film viscosity, film rupture, and roughness factor (if applicable). During high speed operation, oil-film rupture occurs and cavities are formed on the floating-ring inner surface which reduces the effective wetted area. This results in a diminished effective torque and subsequent reduction of ring speed. Surface roughness becomes relevant only when rubbing occurs due to very fine film-clearances. Roughness is ignored for purely fluid-borne floating-ring. In practice, the ring-to-journal speed ratio diminishes with each successive rise in journal speed. This is because the value of $\left(\frac{\mu_2}{\mu_1} \right)$ grows very large as a result of rapid thinning of μ_1 .

IV. EXPERIMENTAL IDENTIFICATION OF DYNAMIC FORCE COEFFICIENTS

The experiment rig consists of a central FRB housing, length 61.0 mm, inner diameter 42.0 mm and outer diameter 100.0 mm, suspended by eight support springs ($K_s = 2.0 \times 10^3 N/m$) Four pairs of adjustable, sliding contact, axial pins projected from the bearing pedestals serve as pitch-stabilizers. At mid-span of the bearing housing a pair of X and Y directed load-platforms takes the impact force. The vertical load-platform also has a provision for static load, linked to a load-cell by a cable coupled with a spring. Two pairs of gap sensors attached orthogonally on the housing measure the floating-ring and the housing displacements. Floating-ring speed and convective oil temperature are measured by an optical sensor and a thermocouple installed axially on the ring-retainer plate respectively. The test shaft is SCM440 of mass 0.948 kg, length 314.0 mm, and diameter 24.0 mm, which runs through the floating-ring and is supported at both ends by twin tandem angular-contact ball bearings in the end-pedestals. An inverter controlled motor of 75 kW and maximum spin-speed of 60,000 rpm drives the rigid shaft via a spline-coupling. Figure 5 presents a well descriptive image and a sectioned schematic of the FRB test-rig.

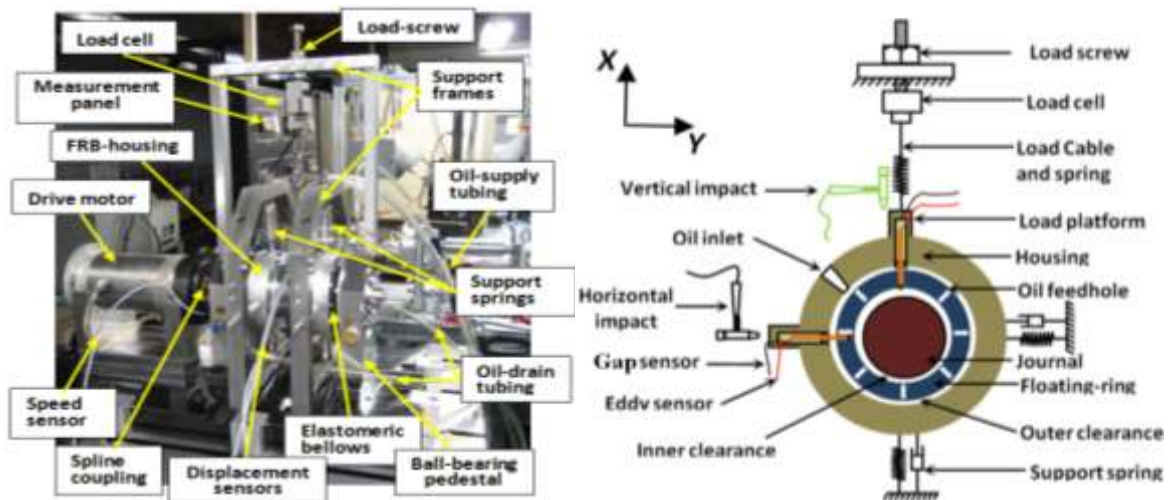


Fig. 5 FRB dynamic force coefficients identification test-rig (image and schematic)

The floating-ring material is UNSC17200 of mass 0.15 kg, overall length 45.00 mm; outer diameter 41.85 mm (clearance of 75 μm from housing) and inner diameter 24.10 mm (clearance of 50 μm from the journal). Table 1 presents details of test-rig parameters. Eight equally spaced identical radial feedholes of diameters 2.80 mm, sunk along the mid-span circumferential groove, serve as ducts for lubricant and convective heat transfer between the two oil-films.

Table 1: Dynamic test-rig parameters and test conditions

Parameters	Value
(a) Floating-ring and journal dimensions	
Inner radial clearance, C_1 [μm]	50
Outer radial clearance, C_2 [μm]	75
Radius ratio of ring, R_2/R_1	1.75
Groove width, b [mm]	3.0
Length of ring, $L=(L_r-b)/2$, [mm]	21
Slenderness ratio, $L/2R_2$	0.5
Oil feedhole diameter, [mm]	2.8
Number of feedholes	6
Mass of ring [kg]	0.15
Mass of housing [kg]	4.06
(b) Specific constants	
Ring thermal expansion [μm/m-°C]	18.4
Journal thermal expansion [μm/m-°C]	17.2
Density of oil [kg/m ³]	862
Viscosity of oil at 40 °C [cSt]	32.1
(c) Sensor specifications	
U8-Gap sensor sensitivity [V/mm]	7.87
U8-Gap sensor resolution [kHz]	70
U8-Gap sensor range [mm]	0.35~2.0
U8-Gap sensor temp. drift [%L/S/°C]	± 0.004

The coefficients of thermal expansion of the chosen journal and ring materials are 17.2 μm/m-°C and 18.4 μm/m-°C, respectively. A heavy duty, *Kixx da* lubricant of density 848 kg/m³, viscosity-index 140, and kinematic viscosities 64.5 mm²/s (at 40°C) and 10.0 mm²/s (at 100°C), respectively is used. Tamunodukobipi, et al [6, 9] presented detailed test procedure, data acquisition technique and post-processing for FRBs.

V. RESULTS AND DISCUSSIONS:

Figure 6 displays the results of both measurement and prediction of FRB stiffness coefficients under a steady load of 100N. All stiffness coefficients increase with rising journal speed except K_{yy} . This is valid because of the improved hydrodynamic wedge at elevated speed. Cross-couple term K_{xy} grows sharply to a gentle slope at 10,000rpm while K_{yx} is almost linear. The initial high negative value of K_{xy} accounts for the wobbling instability motion of the floating-ring and its consequential large sub-synchronous whirl amplitudes prevalent at low journal speed. Observably, the bearing gets more stable beyond 10,000rpm with the cross-coupling coefficients (K_{xy} , K_{yx}) seemingly becoming equal and cancelling out the cross-coupling effects of each other. Also, the improved stability is attributed to a progressive decrease of inner oil-film clearance (i.e. larger C_2/C_1) and the development of a more symmetric hydrodynamic wedge. Consequently, the floating-ring orbital radius is also reduced for speeds greater than 10,000rpm because the supporting outer oil-film grows stiffer: thus, constraining the floating-ring to spin about its rotational axis. The prediction by the 4-*D.O.F* model agrees well with the actual measurement. Calculated measurement uncertainties are: impedance 11.9% , static load 15% and journal speed 1.0%.

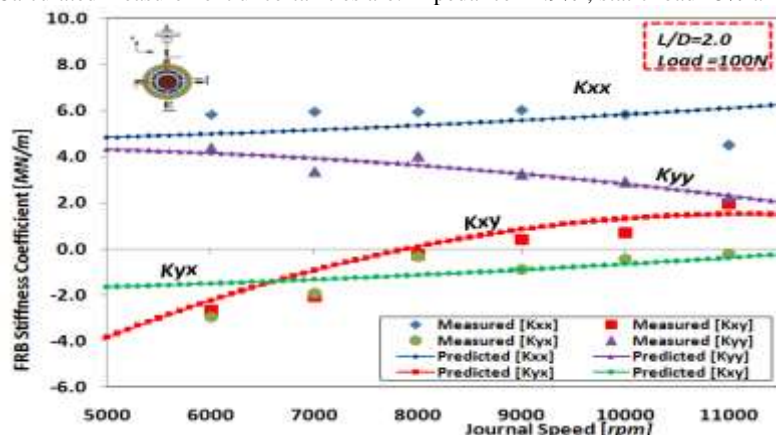


Fig. 6 Stiffness coefficients of FRB with circumferential grooves

In Figure 7, the damping coefficients improve with rising journal speed but at different rates as indicated by the test results. Such phenomenal behavior explains FRB remarkable damping capability and suitability for high speed turbo-machinery. Even when the destabilizing stiffness terms attain large values within the unstable, low speed region [6], the corresponding direct damping is sufficient to prevent total instability. In this case, the predictions fairly match measurements except for the emergence of two non-identical cross-couple damping terms. The identified C_{xy} is fairly insensitive to speed, whereas C_{yx} moves from negative to positive value at higher speed. The trend of the test results agrees with predictions of Chow [8] for $C_2/C_1=1.2$.

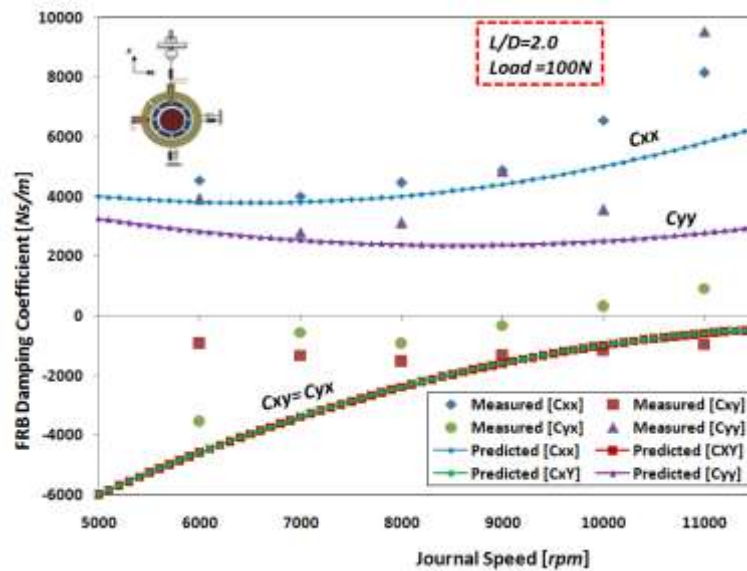


Fig. 7 Damping coefficients of FRB with circumferential grooves

Inertia coefficients derived from test data are almost independent of speed as presented in Figure 8. Conventional theory assumes that the direct inertia terms, M_{xx} and M_{yy} , should equal the physical dynamic mass (the mass total of the housing and the ring); whereas the cross-couple terms are zero. Nevertheless, the total physical mass of the dynamic parts is 4.21 kg which is approximately the mean of M_{xx} and M_{yy} . The magnitude of M_{xx} in the direction of static load is slightly larger than M_{yy} which points in the normal direction. The same discrepancy is observed with the cross-couple terms, M_{xy} and M_{yx} , which average at 1.01 Ns^2/m . This implies that inertia forces (M_{xx} , M_{yy}) directly influenced by the static load are higher than M_{yy} , M_{yx} which are indirectly induced.

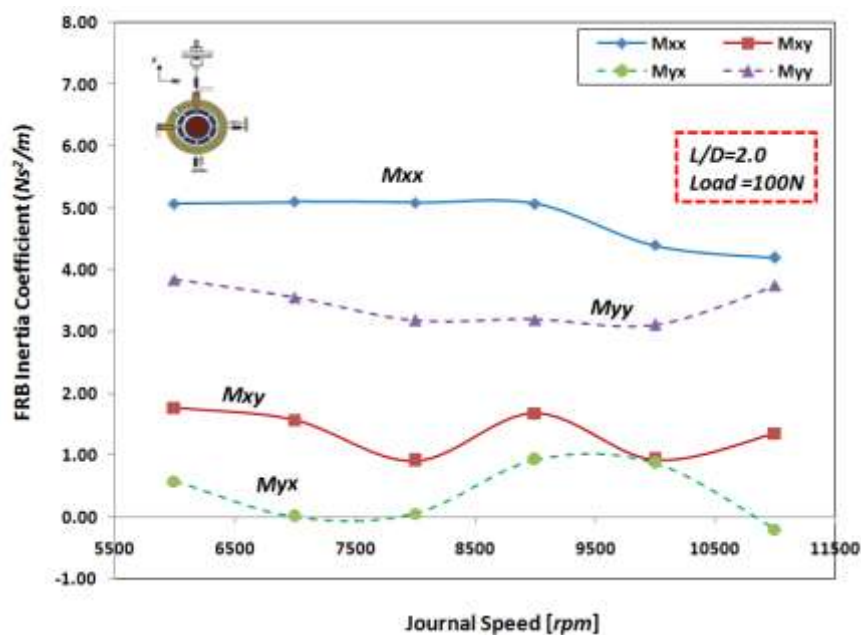


Fig. 8 Inertia coefficients of FRB with circumferential grooves

Figure 9 shows the variation of convective heat dissipation for various loads and speeds. This is imperative because of its impact on the clearance ratio C_2/C_1 and oil viscosity ratio (μ_2/μ_1), which by implication affects the dynamic force coefficients. It is found that thermal growth recorded after 10 minutes of run at each speed maintains a quadratic relationship with incremental journal speed. The gradient becomes moderately smaller when static load is applied because oil agitation due to floating-ring whirl is mitigated. Thermal analysis predicts more than 120% increase in C_2/C_1 and over 600% of μ_2/μ_1 at higher speeds.

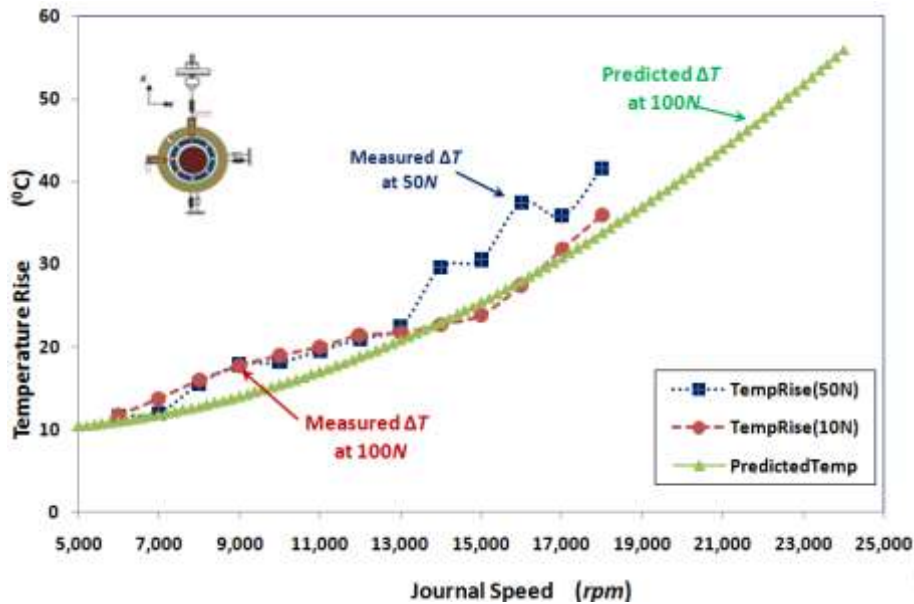


Fig. 9 A plot of the average convective heat loss against journal speed

In Figure 10, the ring-to-journal speed ratios (Ω_R/Ω_J) obtained both by measurement and prediction using Eq. (13) are reasonably in good agreement. The curves begin from points below 0.4 on the y-axis and slope steadily downward as journal speed increases. The rapid thinning of inner film viscosity (i.e. sharp increase of μ_2/μ_1) reduces the torque on the ring's inner surface. The accelerating torque becomes weaker than the decelerating drag on the outer. Thus, the ring-speed ratio drops with successive increase in speed. However, the increase in the value of μ_2/μ_1 and its effect on ring speed ratio gradually become lesser at speeds (> 15,000 rpm). It is also observed that higher static load produces lower Ω_R/Ω_J . The floating-ring motion is retarded because of load induced eccentricity; and boundary interaction. Ring's motion finally freezes under a static load of 200N.

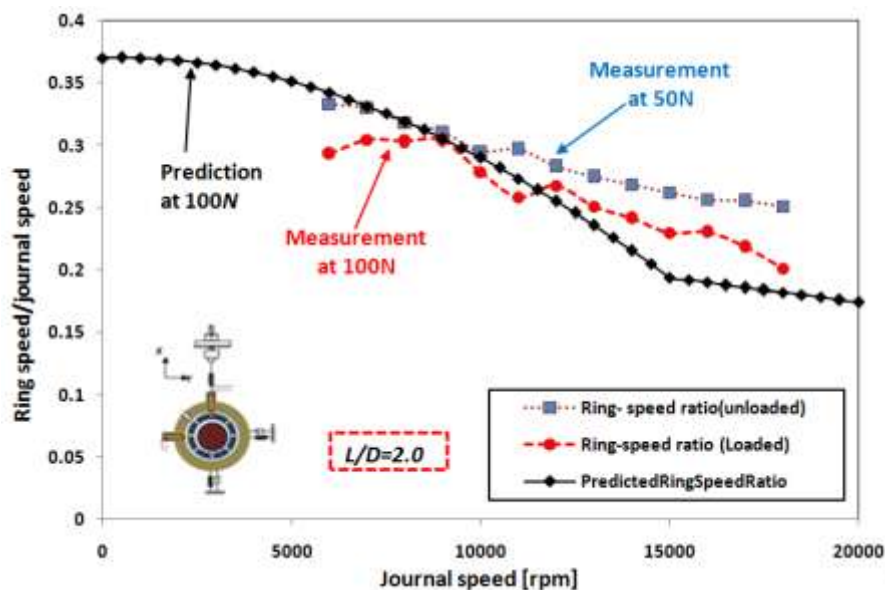


Fig. 9 Plots of the average ring-to-journal speed ratios against journal speed

VI. CONCLUSION

A comprehensive analysis of FRB dynamic behavior is conducted and results presented in comparison with test data. FRB dynamic force characterization is based on a double-film, 4-*D.O.F* model developed and implemented. Also, thermal effects on viscosity ratio, clearance ratio, ring-speed ratio and load capacity are investigated. The investigation shows a general rise in stiffness coefficients with increasing journal speed except K_{yy} which slopes down almost linearly. The low frequency instability is caused by negative destabilizing stiffness K_{xy} , which grows small with rising journal speed. Similarly, all damping terms increase with journal speed but at different rates. C_{xx} and C_{yx} have steeper quadratic slopes than C_{yy} and C_{xy} . Their remarkable rise with journal speed explains the characteristic excellent damping capability and wide application of FRBs in high speed turbo-machinery. The average change in convective oil temperature maintains a fairly quadratic relationship with journal speed. From the analysis, it is found that FRB becomes more stable when the film forces become more symmetric as a result of well-developed outer and inner films. Thermal effect is enormous on μ_2/μ_1 and C_2/C_1 . Hence, a good control of convective heat dissipation is very important for reliable FRB dynamic behavior characterization. FRB parameters identification by measurement is expensive, time-consuming, rigorous, and susceptible to error. Using a well calibrated predictive model, as presented in this work, becomes a panacea to all these snags. The model can be implemented as a stand-alone virtual tool or adopted as a subroutine in a larger program for bearing analysis.

REFERENCES

- [1] Shaw, C., and Nussdorfer, T., 1947, "An Analysis of the Full-Floating Journal Bearing, NACA Report No., 866, pp. 95–107."
- [2] Born, H., 1987, "Analytical and Experimental Investigation of the Stability of the Rotor-Bearing System of a New Small Turbocharger," ASME Paper No.87-GT-110.
- [3] Tanaka, M., 1996, "A Theoretical Analysis of Stability Characteristics of High Speed Floating Bush Bearings," Proc. 6th International Conference on Vibrations in Rotating Machinery, IMechE Conference Transaction 1996–6 _ISBN: 1–86058–009–2_, Oxford, UK, Paper No. C500/087/96, pp. 133–142.
- [4] Holt, C., and San Andrés, L., 2003, "Test Response of a Turbocharger Supported on Floating Ring Bearings—Part I: Assessment of Subsynchronous Motions," Proc. 19th Biennial Conference on Mechanical Vibration and Noise, Chicago, IL, ASME Paper No. DETC 2003/ VIB-48418.
- [5] Holt, C., and San Andrés, L., 2003, "Test Response of a Turbocharger Supported on Floating Ring Bearings—Part II: Comparisons to Nonlinear Rotor-dynamic Predictions," Proc. 19th Biennial Conference on Mechanical Vibration and Noise, Chicago, IL, ASME Paper No. DETC 2003/ VIB-48419.
- [6] Tamunodukobipi, D., Kim, C.H., and Lee, Y.B., 2014, "Dynamic Performance Characteristics of Floating-Ring Bearings with Varied Oil-Injection Swirl-Control Angles," JDSMC of ASME Journals, doi: DS 13-1440
- [7] Tataru, A., 1970, "An Experimental Study on the Stabilizing Effect of Floating Bush Journal Bearings," Bull. JSME, 13, pp. 859–863.
- [8] Chow, C.Y. (1983), "Dynamic characteristics and stability of a helical grooved floating-ring bearing operated in turbulent regime", ASLE Trans., 27(2), 154-163.
- [9] Tamunodukobipi, D., Choe B.S, and Lee, Y.B., 2014, "Feasibility Study of Instability Control of a Floating Ring Bearing for Turbocharger," Proceedings of Asian Congress on Gas Turbines, Seoul, Korea, ACGT2014-0156
- [10] Li, C., 1982, "Dynamics of Rotor Bearing Systems Supported by Floating Ring Bearings," ASME J. Lubr. Technol., 104, pp. 469–477.
- [11] Orcutt, F., and Ng, C., 1968, "Steady-State and Dynamic Properties of the Floating-Ring Journal Bearing," ASME J. Lubr. Technol., 90, pp. 243–253.
- [12] Lund J.W., 1965, Rotor bearings dynamic design technology, part III: Design handbook for fluid film bearings, Mechanical Technology Inc., AFAPL-Tr-65-45-1965.
- [13] Taylor, R. L., 1999, The inclusion of lubricant shear thinning in the short bearing approximation, Proc. Instn Mech. Engrs, Part J: J. Engineering Tribology, 213, 35–46.
- [14] Taylor, R. L., 1999, The inclusion of lubricant shear thinning in journal bearing models. Lubrication at The Frontier. The Role of the Interface and Surface Layers in the Thin Film and Boundary Regime (Ed. D. Dowson), Tribology Series, 36, pp. 611–619.